Capillary-Driven Flow in Open Microchannels Printed with Fused Deposition Modeling

Robert K. Lade Jr.[1], Erik J. Hippchen[1], Luke Rodgers[2], Christopher W. Macosko[1], and Lorraine F. Francis[1]

[1]Department of Chemical Engineering and Materials Science, University of Minnesota
421 Washington Ave. SE, Minneapolis MN, 55455, USA

[2]Stratasys Ltd., 7665 Commerce Way, Eden Prairie, MN, 55344, USA

Abstract

The fundamentals of fluid flow in 3D printed, open microchannels created using fused deposition modeling (FDM) are explored. Printed microchannels are used in microfluidic devices and have potential applications in embedding electronics in plastic substrates. However, FDM parts possess rough surfaces, and in this study, surface topography is shown to have an important impact on flow behavior, causing the liquid to travel down the channel with a characteristic 'pulsing' movement. We also analyze the influence of print orientation on capillary flow, where microchannels printed in specific orientations are shown to exhibit different flow dynamics.

Keywords: Fused deposition modeling ; capillary flow ; microchannel ; flow dynamics

1. Introduction

Fluids are brought into contact with three-dimensional (3D) printed parts for a variety of reasons. For example, liquid coatings are often applied after printing to smooth,[1] seal,[2] strengthen, or add functionality[3] to a part. Additionally, 3D printed microfluidic devices have been used by several researchers[4–6] for a variety of applications; all of these devices involve interfacing fluids with a 3D printed surface. While 3D printing microfluidic devices has become common,[7] little is known about how the 3D printed surface influences the flow dynamics. Because many 3D printing technologies produce parts with rough surfaces,[8–10] the flow dynamics can potentially be more complicated than on flat surfaces.

The increasing number of studies involving direct contact between fluids and 3D printed surfaces merits a more in-depth understanding of the physical principles and dynamics governing this interaction. In this paper, we focus on the fundamentals of fluid flow on parts printed with fused deposition modeling (FDM). Specifically, we look at the behavior of capillary flow in FDM-printed open microchannels. Capillary flow in 3D printed microchannels not only has important applications in microfluidic device design, but also has potential applications in embedding electronics in 3D printed parts.[11] FDM was chosen as an initial 3D printing technology for study due to its flexibility and accessibility.

2. Experimental

2a. Microchannel design and printing

All microchannels were printed using a Dimension 1200es 3D FDM printer (Stratasys, Inc., Eden Prairie, MN). Acrylonitrile butadiene styrene (ABS P-400, Stratasys, Inc.) was used as the model material and a soluble support (P-400SR, Stratasys, Inc.) was used as the support

material. All microchannels were printed with a layer resolution of 254 µm (0.01 in.) with solid interior fill and default temperature settings.

A cartoon of one of the CAD designs is shown in Fig. 1a and a printed capillary filled with liquid is shown in Fig. 1b. Each capillary consists of one reservoir connected to a channel, with widths ranging from 80 - 750 µm and depths of 250 µm. Reservoir diameters were designed such that the reservoir and channel volumes were equal.

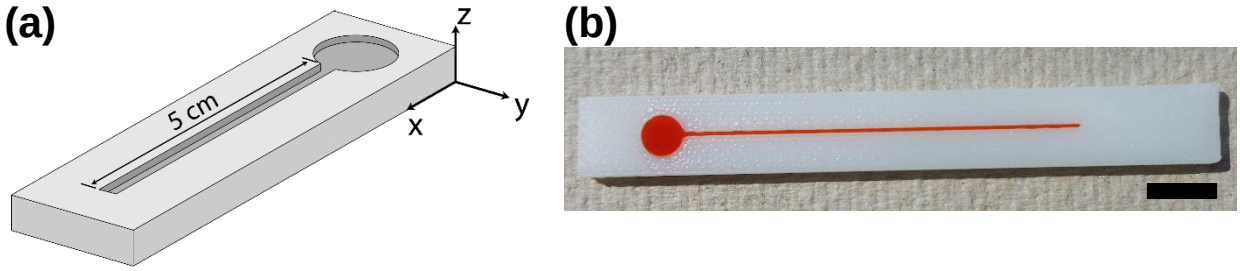

Figure 1. (a) Cartoon of microchannel CAD design. Not to scale. (b) Coated capillary printed from a CAD design specifying a 400 µm wide channel. Channel is filled with water with red dye. Scale bar: 1 cm.

Each part was printed in one of three orientations (Fig. 2a). Because FDM employs cylindrical strands of material, FDM parts have a characteristic rough surface. Accordingly, each orientation imparts a unique topography to the bottom of the microchannel. Capillaries oriented at 45° and 135° have channels which are oriented parallel with and perpendicular to the printed layer beneath it, respectively. Figs. 2b-d shows cross sections (parallel to the length of the channel) of microchannels printed in each orientation. The microchannel geometries illustrated in Figs. 2b, c, and d will henceforth be referred to as diagonal, parallel, and perpendicular orientations, respectively.

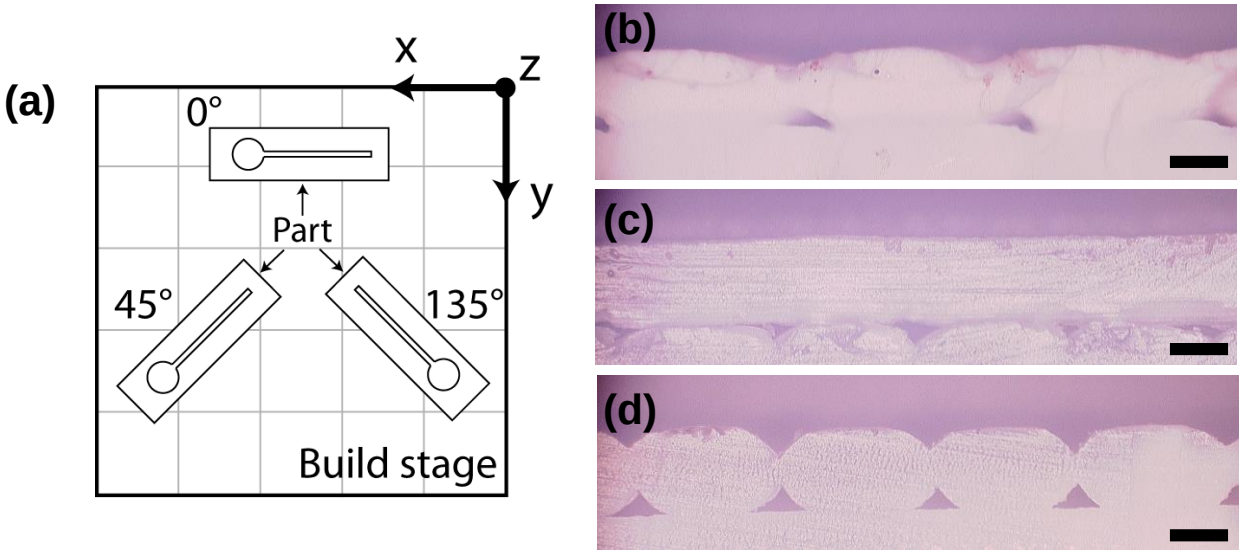

Figure 2. (a) Cartoon of microchannel part rotated 0°, 45°, and 135° on build stage. During printing, the print head rasters back and forth at 45° in the x-y plane. Cross sections (parallel to the length of the channel) of microchannels printed in (b) diagonal (0°), (c) parallel (45°), and (d) perpendicular (135°) orientations. Scale bars: 200 µm.

2b. Microchannel surface treatment

After printing, microchannels were coated with an ultraviolet (UV) curable adhesive (NOA73, Norland Products, Inc., Cranbury, NJ) to make the channel watertight. Before coating, each capillary was washed with water, air dried, and plasma treated. After plasma treatment, a foam brush (model no. 8500 0100, Home Depot, Atlanta, GA) was used to apply the coating over the entire part. The adhesive was then cured under long-wave UV light (366 nm) for 45-60 minutes.

2c. Monitoring capillary flow

Capillary flow was monitored using a digital optical microscope (KH-7700, Hirox USA, Hackensack, NJ) at 50x zoom. The test liquid was an aqueous solution of 84 wt. % glycerol mixed with 40 µL of blue food dye per 20 mL of glycerol solution. The viscosity and surface tension of the test solution was ~80 mPa·s and 62 mN/m, respectively, and its contact angle with the coated ABS was ~40°. Prior to each experiment, each capillary was plasma treated to encourage wetting and spreading. After dispensing the glycerol solution into the reservoir, videos of the flow were recorded and the position of the capillary front in each frame was extracted using ImageJ software (v1.48v, NIH).

3. Results and Discussion

3a. Microchannel geometry and surface topography

A sample cross section of a microchannel is shown in Fig. 3, taken perpendicular to the length of the channel. Microchannel walls are formed by individual printed strands, giving each microchannel a characteristic rounded shape. Although print orientation does not affect the shape of the microchannel, it does affect print accuracy. Microchannel dimensions were determined using optical microscopy and, in general, microchannels printed in a parallel orientation match their CAD designs most closely. In all orientations, wider microchannels are printed more accurately. Microchannel depth was relatively consistent across all orientations, with an average value of 260 ± 30 µm.

Figure 3. Cross section of FDM microchannel, perpendicular to the length of the channel. Scale bar: 200 µm.

The surface topography of the microchannels printed in each orientation is shown in Figs. 2b-d. While both the diagonal and perpendicular print orientations present the liquid with relatively large topographical obstacles during flow down the channel, the parallel orientation presents a relatively smooth surface. The impact that these topographies have on the capillary flow will be discussed in the next two sections.

3b. Capillary flow dynamics

The FDM microchannels explored in this study exhibited unique flow dynamics. Fig. 4 shows a representative plot of meniscus (i.e., capillary front) position vs time for a microchannel of width ~300 µm printed in a diagonal orientation. The most distinguishing feature of this flow is the small jump in position every 0.5 - 1s. Instead of flowing smoothly down the channel, the flow exhibits a characteristic "pulsing" motion as a result of the surface topography. As the meniscus approaches a trough between two printed strands (see Fig. 2b), it becomes pinned for a short time. Once that pinning is overcome, the meniscus then surges forward quickly due to this build up liquid, with the edge that became pinned first becoming unpinned first.

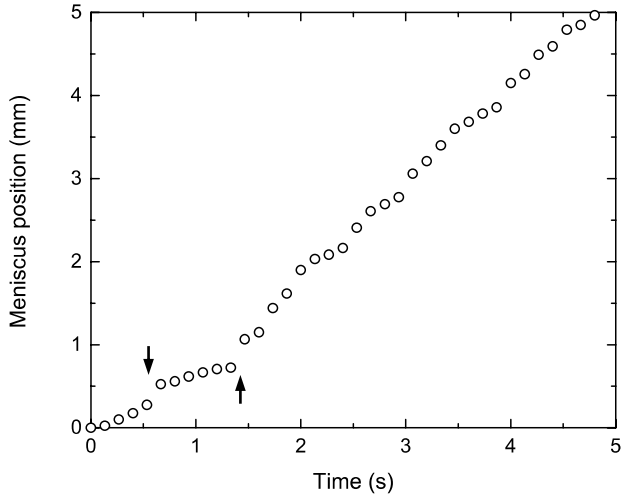

Figure 4. Meniscus position vs time for a microchannel with width of 320 µm, printed in a diagonal orientation. Jumps in position occur every 0.5 – 1 s. Arrows indicate some of these jumps.

This pulsing flow continues down the entire channel, with pinning time varying from trough to trough, corresponding to small variations that arise during printing. For example, in Fig. 4 it is clear that after about 0.5 s, the liquid became pinned for a relatively long time (~ 1 s) before it started to flow again whereas the pinning visible at 2 s lasts less than 0.5 s. Arrows indicate the jumps that occur before and after the pinning around 1 s. Thinner capillaries were observed to exhibit shorter pinning times and hence an overall smoother flow, while in larger capillaries the pulsing flow was more pronounced.

3c. Effect of print orientation

Capillaries printed in a perpendicular orientation exhibit a strong, uniform pulsing flow. This is due to the topography being completely perpendicular to the flow such that neither the top nor the bottom of the meniscus becomes unpinned first. This feature results in a slightly longer pinning of the meniscus and a proportionally faster pulse upon depinning. Oppositely, microchannels printed in a parallel orientation exhibit no pulsing. Because there are essentially no topographical barriers along the length of the channel (see Fig. 2c), the flow can proceed uninterrupted.

Despite the vastly different flow dynamics that each capillary orientation imparts to the liquid flowing down it, the average measured velocity was observed to be essentially independent of print orientation. This result suggests that the surges that occur at each trough on the diagonally

and perpendicularly oriented capillaries offset the slowing down caused by the pinning essentially equally, resulting in no net effect on the average velocity as it moves down the microchannel. Flow velocity was observed to increase as channel width decreased. At the smallest printable channel size (~200 μm), flow velocities around 1000 μm/s were recorded. At the largest widths tested (~700 μm), flow velocities around 200 μm/s were recorded.

4. Summary and future work

In this work, we showed that due to the nature of the FDM printing process, printed microchannels have a topography that depends on orientation. This topography causes the capillary flow to move with a pulsating motion, resulting from a constant pinning and depinning at each topographical feature. Despite this unique motion, the average velocity of the flow is not affected by differences in the topography. When printing microchannels, the minimum feature sizes are set by the individual capabilities of the printer. Here, we were able to achieve minimum channel depths and widths of approximately 250 μm and 200 μm, respectively.

Future work will focus more on a quantitative understanding of the flow dynamics in each differently oriented microchannel. Although FDM is a relatively simple and accessible printing technology, other technologies with higher resolution may offer better opportunities for printing microchannels. Future work will focus on comparing the FDM microchannels in this study to microchannels printed using stereolithography. This work provides a foundation for developing a more in-depth understanding of the fundamentals governing flow in 3D printed microfluidic devices and also promises to promote the development of other applications involving microchannels embedded in 3D printed parts.

5. Acknowledgements

The authors would like to thank the industrial supporters of the Coating Process Fundamentals Program (CPFP) of the Industrial Partnership for Research in Interfacial and Materials Engineering (IPRIME) for supporting this research. This work was also supported by funding through MnDRIVE. Parts of this work were carried out at the Minnesota Nano Center, which receives partial support from NSF through the NNIN program. The authors would like to extend their gratitude to Satish Kumar at the University of Minnesota for helpful discussions.

6. References

(1) Zhu, J.; Chen, J.; Lade Jr., R.K.; Suszynski, W.J.; Francis, L.F. Water-Based Coatings for 3D Printed Parts. *J. Coatings Technol. Res.* **2015**. doi: 10.1007/s11998-015-9710-3.

(2) Mireles, J.; Adame, A.; Espalin, D.; Medina, F.; Winker, R.; Hoppe, T.; Zinniel, B.; Wicker, R. Analysis of Sealing Methods for FDM-Fabricated Parts. Technical report, W.M. Keck Center for 3D Innovation. The Univ. of Texas, El Paso (2011).

(3) Zhu, J. Water-Based Antimicrobial Coating for 3D Printed Medical Devices. Stratasys White Paper. Available at: http://web.stratasys.com/rs/objet/images/SSYS-WP-3DP-AntimicrobialCoating-06-20-14%20FINAL.pdf (Accessed July 16, 2015).

(4) Anderson, J.R.; Chiu, D.T.; Jackman, R.J.; Chemiavskaya, O.; McDonald, J.C.; Wu, H.; Whitesides, S.H.; Whitesides, G.M. Fabrication of Topologically Complex Three-Dimensional Microfluidic Systems in PDMS by Rapid Prototyping. Anal. Chem. 2000, 72, 3158–3164.

(5) Erkal, J.L.; Selimovic, A.; Gross, B.C.; Lockwood, S.Y.; Walton, E.L.; McNamara, S.; Martin, R.S.; Spence, D.M. 3D Printed Microfluidic Devices with Integrated Versatile and Reusable Electrodes. Lab Chip 2014, 14, 2023–32.

(6) Bhargava, K.C.; Thompson, B.; Malmstadt, N. Discrete Elements for 3D Microfluidics. Proc. Natl. Acad. Sci. 2014, 111, 15013–15018.

(7) Gross, B.C.; Erkal, J.L.; Lockwood, S.Y.; Chen, C.; Spence, D.M. Evaluation of 3D Printing and Its Potential Impact on Biotechnology and the Chemical Sciences. Anal. Chem. 2014, 86, 3240-53.

(8) Fischer, M.; Schöppner, V. Some Investigations Regarding the Surface Treatment of Ultem* 9085 Parts Manufactured with Fused Deposition Modeling. In Proceedings of the Solid Freeform Fabrication Symposium; Austin, TX, 2013; pp. 805–815.

(9) Stampfl, J.; Liska, R. New Materials for Rapid Prototyping Applications. Macromol. Chem. Phys. 2005, 206, 1253–1256.

(10) Hedges, M.; Marin, A. B. 3D Aerosol Jet ® Printing - Adding Electronics Functionality to RP / RM. DDMC 2012 Conf. 2012, 1–5.

(11) Mahajan, A.; Hyun, W.J.; Walker, S.B.; Lewis, J.A.; Francis, L. F.; Frisbie, C. D. High-Resolution, High-Aspect Ratio Conductive Wires Embedded in Plastic Substrates. ACS Appl. Mater. Interfaces 2015, 7, 1841–1847.